The Astrophysical Journal, 837:21 (8pp), 2017 March 1 https://doi.org/10.3847/1538-4357/aa5df4

Evidence for Relativistic Disk Reflection in the Seyfert 1h Galaxy/ULIRG IRAS 05189–2524 Observed by *NuSTAR* and *XMM-Newton*

Yanjun Xu[1], Mislav Baloković[1], Dominic J. Walton[1,2,3], Fiona A. Harrison[1], Javier A. García[1,4,5,8], and Michael J. Koss[6,7,9]
[1] Cahill Center for Astronomy and Astrophysics, California Institute of Technology, Pasadena, CA 91125, USA
[2] Jet Propulsion Laboratory, California Institute of Technology, Pasadena, CA 91109, USA
[3] Institute of Astronomy, University of Cambridge, Madingley Road, Cambridge CB3 0HA, UK
[4] Harvard-Smithsonian Center for Astrophysics, 60 Garden Street, Cambridge, MA 02138, USA
[5] Remeis Observatory & ECAP, Universität Erlangen-Nürnberg, Sternwartstrasse 7, D-96049 Bamberg, Germany
[6] Institute for Astronomy, Department of Physics, ETH Zurich, Wolfgang-Pauli-Strasse 27, CH-8093 Zurich, Switzerland
[7] Institute for Astronomy, University of Hawaii, 2680 Woodlawn Drive, Honolulu, HI 96822, USA
Received 2016 November 4; revised 2017 January 31; accepted 2017 January 31; published 2017 February 28

Abstract

We present a spectral analysis of the *NuSTAR* and *XMM-Newton* observations of the Seyfert 1h galaxy/ULIRG IRAS 05189–2524 taken in 2013. We find evidence for relativistic disk reflection in the broadband X-ray spectrum: a highly asymmetric broad Fe Kα emission line extending down to 3 keV and a Compton scattering component above 10 keV. Physical modeling with a self-consistent disk reflection model suggests that the accretion disk is viewed at an intermediate angle with a supersolar iron abundance, and a mild constraint can be put on the high-energy cutoff of the power-law continuum. We test the disk reflection modeling under different absorption scenarios. A rapid black hole spin is favored; however, we cannot place a model-independent tight constraint on the value. The high reflection fraction ($R_{\rm ref} \simeq$ 2.0–3.2) suggests that the coronal illuminating source is compact and close to the black hole (lying within 8.7 $R_{\rm g}$ above the central black hole), where light-bending effects are important.

Key words: accretion, accretion disks – black hole physics – galaxies: active – galaxies: individual (IRAS 05189–2524) – galaxies: Seyfert – X-rays: galaxies

1. Introduction

The hard X-ray continuum emission of active galactic nuclei (AGNs) is believed to be produced in the corona via thermal Comptonization of ultraviolet (UV) radiation from the accretion disk (e.g., Haardt & Maraschi 1993). This continuum emission is subsequently reprocessed by dense material from either the accretion disk or distant structures such as the dusty torus or the broad-line region (BLR), producing the characteristic reflected X-ray spectrum (e.g., George & Fabian 1991). Fluorescent spectral lines, line edges, and a Compton hump are typical features of the reflected X-ray spectrum. Fe Kα is the most prominent spectral line in the X-ray band, due to its high cosmic abundance and fluorescent yield. The line emission from the innermost regions of the accretion disk is relativistically broadened by the combined effects of Doppler shifts and gravitational redshift (Fabian et al. 1989; Laor 1991), which skew the line profile into an extended red wing. Assuming that the accretion disk extends down to the innermost stable circular orbit (ISCO), which is determined by the spin of the black hole (BH), a relativistically broadened Fe Kα line could be used as a probe of the BH spin.

So far, broad Fe Kα lines have been detected in many AGNs (e.g., Tanaka et al. 1995; Nandra et al. 2007; Risaliti et al. 2013; Walton et al. 2013); these are mostly Seyfert 1–1.5 galaxies, with only a few absorbed Seyfert 2 galaxies showing such features, e.g., IRAS 18325–5926 (Iwasawa et al. 1996) and IRAS 00521–7054 (Tan et al. 2012). *XMM-Newton* and *Suzaku* observations of IRAS 00521–7054 revealed a possibly strong and broad Fe Kα line favoring a high BH spin; however, the broad line could also be artificially produced by a combination of partial covering absorbers (Tan et al. 2012; Ricci et al. 2014). With high-quality broadband X-ray data and multiepoch observations, BH spins have been robustly constrained in some nearby obscured Seyferts (e.g., Seyfert 1.9 galaxy NGC 1365; Risaliti et al. 2013; Walton et al. 2014), but the measurement is still difficult for these obscured objects.

IRAS 05189–2524 is an ultraluminous infrared galaxy (ULIRG) with $\log(L_{\rm IR}/L_{\odot}) = 12.16$ (U et al. 2012) and hosts a Compton-thin AGN at redshift $z = 0.0426$. While originally classified as Seyfert 2 (Veilleux et al. 1995), broad polarized Balmer lines were detected (Young et al. 1996), and near-infrared spectroscopy revealed broad Paschen lines (Veilleux et al. 1999; Severgnini et al. 2001), indicating the existence of a hidden BLR. Therefore, it has been more accurately classified as a hidden broad-line Seyfert 1 galaxy (Seyfert 1h galaxy/S1h; Véron-Cetty & Véron 2006), which defines the kind of Seyfert 2s having the spectra of Seyfert 1s in the polarized light.

In the X-ray band, IRAS 05189–2524 is one of the most luminous ULIRGs in the sky, which are typically merger systems undergoing rapid star-forming activities. IRAS 05189–2524 is likely a late-stage merger of two spiral galaxies (Sanders et al. 1988). Its X-ray emission is dominated by the central AGN rather than starburst activities (Veilleux et al. 1999). Iron emission has been detected in IRAS 05189–2524 from previous X-ray observations by *BeppoSAX* (Severgnini et al. 2001) and *Suzaku* (Teng et al. 2009), but the general line profile was not resolved. The source went through a major spectral change during the 2006 *Suzaku* observation when the 2–10 keV flux dropped by a factor of ~30, which could be explained by an increase in the

[8] Alexander von Humboldt Fellow.
[9] SNSF Ambizione Fellow.

absorption column density or the change of the intrinsic AGN luminosity (Teng et al. 2009). At a galactic scale, high-velocity outflows of ionized (Westmoquette et al. 2012; Bellocchi et al. 2013), neutral (Rupke et al. 2005; Teng et al. 2013; Rupke & Veilleux 2015), and molecular (Veilleux et al. 2013) gas have been observed.

Outflows have been recognized as a signature of AGN feedback, which is believed to play an important role in the coevolution of AGNs and their host galaxies. Evidence for multiphase outflowing gas has been observed in AGNs on a wide rage of spatial scales from that of the central accretion disk to large-scale molecular outflows. If outflows at different scales are all AGN driven, linking them could help unveil the expansion mechanism of the wind; such studies have been conducted on ULIRGs IRAS 11119+3257 (Tombesi et al. 2015) and Mrk 231 (Feruglio et al. 2015). In the X-ray band, there is growing evidence for ultrafast outflows (UFOs) with the typical velocities of $\sim 0.1c$–$0.2c$, detected by fitting blueshifted Fe K-shell absorption lines between 7 and 10 keV (e.g., Pounds et al. 2003; Tombesi et al. 2010; Pounds & King 2013). In the case of PDS 456, a P-Cygni-like profile was observed, demonstrating a powerful wide-angle outflow (Nardini et al. 2015).

In this paper, we report evidence for relativistic disk reflection in IRAS 05189–2524 based on analysis of the broadband X-ray spectrum from *NuSTAR* and *XMM-Newton*. In Section 2, we describe the observations and the data reduction. Section 3 provides the details of our spectral fitting. We present a discussion of the results in Section 4 and summarize our results in Section 5.

2. Data Reduction

IRAS 05189–2524 was observed with *NuSTAR* (Harrison et al. 2013) and *XMM-Newton* (Jansen et al. 2001) in 2013 as a part of the *NuSTAR* ULIRG survey (Teng et al. 2015) and the *NuSTAR* survey of *Swift*/BAT AGNs (M. Baloković et al. 2017, in preparation). *NuSTAR* observed the source at two epochs: on 2013 February 20 (ObsID 60002027002) and on 2013 October 2 (consecutive ObsIDs 60002027004 and 60002027005), with exposures of 23.1, 25.4, and 8.3 ks, respectively. The *XMM-Newton* observation (ObsID 0722610101) with an exposure time of 37.8 ks was coordinated with the second *NuSTAR* observation. The data set was previously analyzed in the *NuSTAR* ULIRG survey (Teng et al. 2015), with the focus on uncovering the obscuration levels and intrinsic luminosities of several nearby ULIRGs. We reduced the data following the data processing description in Teng et al. (2015).

2.1. NuSTAR

The *NuSTAR* data were processed using v.1.6.0 of the NuSTARDAS pipeline with *NuSTAR* CALDB v20160731. For each observation, the source spectra were extracted at the position of IRAS 05189–2524 within the radius of 60″. Corresponding background spectra were extracted from source-free areas on the same chip using polygonal regions. As discussed in Teng et al. (2015), the *NuSTAR* data show minor count rate variability (∼20%) and no obvious change in spectral shape between the two epochs. Therefore, we combined the three *NuSTAR* observations using the ADDSPEC script in HEASoft v6.19 to maximize the signal-to-noise ratio (S/N) of the spectra. We binned the data taking into account the background level to provide a nearly constant S/N over the *NuSTAR* bandpass, with a minimum S/N of 3 and median S/Ns of 5.5 and 5.3 for the two focal plane modules (FPMA and FPMB, respectively).

Table 1
XSPEC Models

Model	XSPEC Components	Spectral Range (keV)
1	zpcfabs*powerlaw + mekal	0.3–30
2	zpcfabs*(pexrav + zgauss) + mekal	0.3–30
3a	zpcfabs*relxilllp	2–30
3b	(partcov*tbnew_feo)*relxilllp	2–30
4a	zpcfabs*XSTAR*relxilllp	2–30
4b	(partcov*tbnew_feo)*XSTAR*relxilllp	2–30

2.2. XMM-Newton

The *XMM-Newton* observation was reduced with the *XMM-Newton* Science Analysis System v14.0.0 following standard procedures. The raw event files were filtered using EPCHAIN and EMCHAIN to produce cleaned event lists for each of the EPIC-pn (Strüder et al. 2001) and EPIC-MOS (Turner et al. 2001) detectors, respectively. Science products were then produced using XMMSELECT, considering only single and double events for EPIC-pn, and single to quadruple events for EPIC-MOS. We extracted the source from a circular region of radius 40″, while background was estimated from a large region of blank sky on the same detector as IRAS 05189–2524. Instrumental response files were generated with RMFGEN and ARFGEN for each detector. The good exposure is ∼31 ks for EPIC-pn and ∼36 ks for each of the two EPIC-MOS detectors. After performing the reduction separately for MOS1 and MOS2, we combined these data into a single spectrum using ADDASCASPEC. The MOS and PN spectra were grouped to have 25 counts per bin.

3. Spectral Analysis

We model the time-averaged *NuSTAR* and *XMM-Newton* spectra jointly in XSPEC v12.9.0 (Arnaud 1996) using the χ^2 statistics. All uncertainties of the spectral parameters are reported at the 90% confidence level. Cross-normalization constants are allowed to vary freely for *NuSTAR* FPMB and *XMM-Newton* MOS and PN and are assumed to be unity for FPMA. The values are within ∼10% of unity, as expected from Madsen et al. (2015). For all the spectral fitting, we take into account the Galactic absorption by modifying the spectrum with a `TBabs` absorption model (Wilms et al. 2000). The Galactic column density is set to $N_{\rm H,gal} = 1.66 \times 10^{20}$ cm^{-2} (Kalberla et al. 2005).

We begin our spectral analysis of the broadband X-ray spectrum considering the band from 0.3 to 30 keV, as it becomes background dominated above 30 keV. We first fit the spectrum with a power-law model subject to one partial covering neutral absorber modeled with `zpcfabs`, plus a `mekal` line emission model with its elemental abundances fixed at solar values (model 1; XSPEC models are listed in Table 1). The `mekal` component is used to model the thermal plasma contribution from the host galaxy. We find the best fit (reduced chi-square χ^2/dof = 1425.8/1049) with a photon index $\Gamma = 2.29 \pm 0.04$ and a `mekal` temperature

Table 2
Spectral Fitting of IRAS 05189–2524: Absorbed Power-law Model and Phenomenological Reflection Model

Component	Parameter	Model 1	Model 2
ZPCFABS	$N_{\rm H}$ ($\times 10^{22}$ cm^{-2})	$8.82^{+0.27}_{-0.26}$	8.30 ± 0.21
	$f_{\rm abs}$ (%)	$98.89^{+0.08}_{-0.09}$	99*
POWER-LAW	Γ	2.29 ± 0.04	…
MEKAL	kT (keV)	$0.092^{+0.010}_{-0.005}$	$0.087^{+0.006}_{-0.009}$
PEXRAV	Γ	…	2.47 ± 0.04
	$R_{\rm ref}$	…	$1.48^{+0.53}_{-0.44}$
ZGAUSS	LineE (keV)	…	6.40*
	σ (keV)	…	$0.71^{+0.13}_{-0.11}$
	χ^2/dof	1425.8/1049	1194.8/1047

Note. Model 1 and model 2 fit the 0.3–30 keV broadband spectrum from *NuSTAR* and *XMM-Newton*. Parameters with an asterisk are fixed values.

$kT = 0.092^{+0.010}_{-0.005}$ keV. The covering fraction of the neutral absorber is well constrained as 98.89%; therefore, the contribution from the scattered power-law component is negligible above ~2 keV. For simplicity, we fix the value at 99% from here on.

The data/model ratio plot shows strong signatures of disk reflection (Figure 1(b)): a broad iron line peaking around 6.7 keV in the source rest frame with a skewed shape extending down to ~3 keV and residuals above 10 keV from the Compton reflection. In addition, there are possible absorption features of blueshifted Fe K lines in both the *NuSTAR* and the *XMM-Newton* spectra, with the most evident absorption troughs lying in the vicinity of the Fe K edge around 7.3 keV (Figure 2).

3.1. Phenomenological Reflection Model

We then test fitting the reflection features with a phenomenological model by adding a neutral reflection component `pexrav` (Magdziarz & Zdziarski 1995) and one Gaussian emission line with variable width using the model `zgauss` (model 2; see Table 1). We freeze the centroid of the Gaussian emission line at 6.4 keV, the disk inclination angle at the default value (`cos i` = 0.45), and the iron abundance at solar and include no high-energy cutoff (`foldE` = 0), as this simple model is not sensitive to these parameters. The fit is improved considerably with $\Delta\chi^2/\Delta{\rm dof} = -231/-2$ (the best-fit parameters are listed in Table 2). A broad Gaussian line with line width $\sigma = 0.71^{+0.13}_{-0.11}$ keV and equivalent width (EW) $\simeq$ 0.60 keV is required to provide a decent fit for the iron line emission feature in the spectrum. However, a clear excess still remains in the residuals between 3 and 6 keV, as would be expected from the red wing of a relativistically broadened iron line (Figure 1(c)). Model 2 also gives a very steep power law of $\Gamma = 2.47 \pm 0.04$. We do not attempt to interpret the intrinsic continuum steepness at this point, as this is only a phenomenological model.

We note that for both the simple absorbed power-law and the phenomenological reflection model, at least two extra emission features are present in the residuals around 0.9 and 1.9 keV. The 0.9 keV excess might be associated with O Lyα or Fe–L shell emissions, and the feature around 1.9 keV could be caused by ionized Si emission lines. The excesses cannot be adequately fitted with simple Gaussian emission line models, as they could

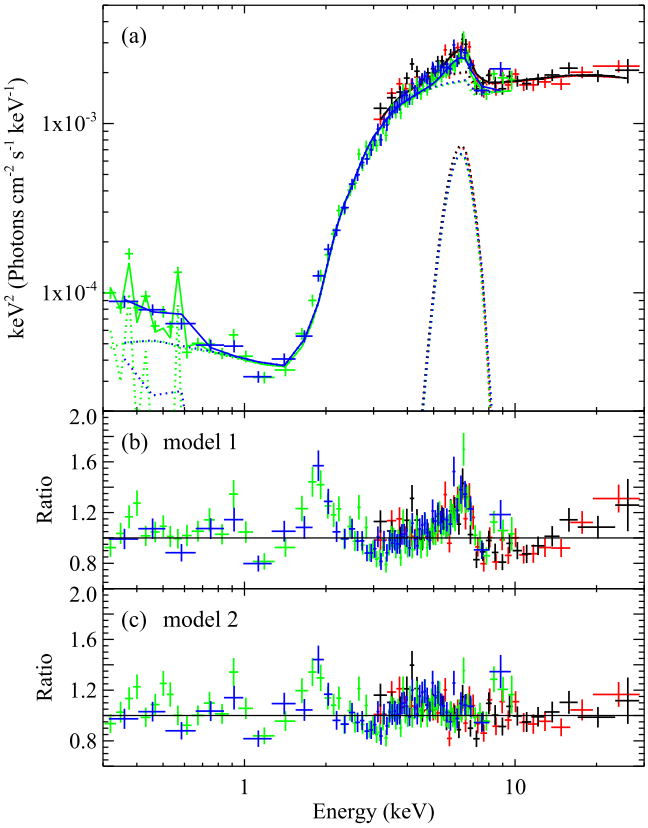

Figure 1. (a) *XMM-Newton* PN (green) and MOS (blue) and *NuSTAR* FPMA (red) and FPMB (black) spectra of IRAS 05189–2524, with the best-fit phenomenological reflection model (model 2). (b) Data/model ratio after fitting an absorbed power law plus a soft `mekal` component to the 0.3–30 keV spectrum (model 1). (c) Residuals of the phenomenal reflection model (model 2). The data are rebinned for display clarity.

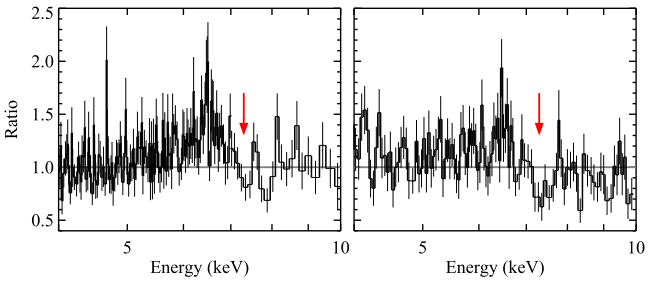

Figure 2. Possible absorption features between 7 and 8 keV marked by arrows in the residual plots of the absorbed power-law model (model 1). Left panel: *XMM-Newton* PN spectrum; right panel: *NuSTAR* FPMB spectrum.

be a complicated combination of ionized absorption, overabundant metal lines, and X-ray contribution from the high-mass X-ray binary population in the star-forming regions. X-ray point-source emission correlates with galaxy star formation rate (SFR) in star-forming galaxies (Lehmer et al. 2010). At an SFR of ~80 $M_\odot$ yr^{-1} (Westmoquette et al. 2012), the 2–10 keV luminosity from the binary population is estimated to be 1.4×10^{41} erg s^{-1}, about 1% of the total luminosity, which is enough to dominate the soft emission of IRAS 05189–2524. Therefore, the soft part of the spectrum likely helps little to constrain the X-ray continuum from the AGN. In order to avoid the possible situation where the soft emission from the host galaxy is driving our modeling of the disk reflection features, we ignore the data below 2 keV from here on.

3.2. Self-consistent Disk Reflection Models

In Teng et al. (2015), the authors attempted to explain the reflection features observed in IRAS 05189–2524 by neutral reflection from the torus, which is commonly the case for Compton-thick AGNs. However, they found that neither the `MYTorus` (Murphy & Yaqoob 2009) nor `the BNTorus` model (Brightman & Nandra 2011) could provide an adequate fit for the broadband spectrum, which ruled out the possibility of distant reflection. In order to explore the relativistic reflection hypothesis, we replace the `pexrav` and `zgauss` components in the phenomenological model with the self-consistent relativistic reflection model `relxill` (Dauser et al. 2014; García et al. 2014) (model 3a; see Table 1). We use `relxilllp` in the `relxill` model family; instead of using an empirical emissivity law, the emissivity is calculated directly in the lamppost geometry (Dauser et al. 2013). `Relxilllp` calculates a self-consistent reflection fraction. This could help us constrain the BH spin by shrinking the parameter space, as results with unphysical solutions of low BH spins with high reflection fractions can be ruled out by the assumption of a lamppost geometry (for discussion, see Dauser et al. 2014). In order to measure the BH spin, we assume that the inner disk radius extends down to the ISCO. We fix the outer radius at the default value of 400 R_g ($R_g \equiv GM/c^2$ is the gravitational radius), as the model is not sensitive to this parameter, and the cutoff energy is allowed to vary in the fitting.

The `relxilllp` model yields a good fit to the 2–30 keV spectrum with $\chi^2/\mathrm{dof} = 862.0/859$ and no obvious excess in the residuals (Figure 3(b)). The intrinsic X-ray continuum is steep, with the power-law photon index $\Gamma = 2.04^{+0.02}_{-0.03}$. It is in the upper range of the photon index distribution observed in local Seyfert galaxies (e.g., Nandra & Pounds 1994; Winter et al. 2009; Rivers et al. 2013), but less extreme than the previously published values for IRAS 05189–2524: e.g., $\Gamma = 2.68^{+0.30}_{-0.13}$ (Teng et al. 2009), $\Gamma = 2.51 \pm 0.02$ (Teng et al. 2015). Albeit lacking high-quality data above 30 keV, the model is able to put a modest constraint on the high-energy cutoff $E_{\rm cut} = 55^{+10}_{-7}$ keV, as discussed in García et al. (2015a); such sensitivity could come partly from the low-energy part of the reflection spectrum (<3 keV). The location of the primary radiation source is found to be close to the disk $h = 2.39^{+0.80}_{-0.32}\ R_g$, with a rapid BH spin (dimensionless spin parameter $a = 0.96^{+0.02}_{-0.03}$), and the self-consistent reflection fraction derived by the model is high ($R_{\rm ref} = 3.24$). The best-fit results also find an intermediate inclination of $\theta = 42° \pm 2°$ and an ionization parameter[10] $\log \xi = 3.02 \pm 0.02$ erg cm s^{-1} for the accretion disk. We note that the iron abundance $A_{\rm Fe}$ is unusually high, with the best-fit value hitting the upper bound of the model of 10. But if we fix the iron abundance at solar in the `relxilllp` model, the fitting degrades considerably ($\Delta\chi^2 \sim 130$), with a visible excess in the Fe K band.

A supersolar metal abundance is not uncommon among ULIRGs (e.g., Rupke et al. 2008). In the case of IRAS 05189–2524, based on the diagnostics of [N II]/Hα, [S II]/Hα, and [O I]/Hα line ratios, an uncommonly high metallicity[11] (>4 $Z_\odot$) is estimated for the outer galactic disk, or else some peculiar ionization effects are needed to explain the line ratio measurements (Westmoquette et al. 2012). If the metallicity is indeed high on the galactic scale in IRAS 05189–2524, it is more physically consistent to use neutral absorption models with supersolar abundances in our spectral fitting, as neutral absorbers normally reside far from the central BH.

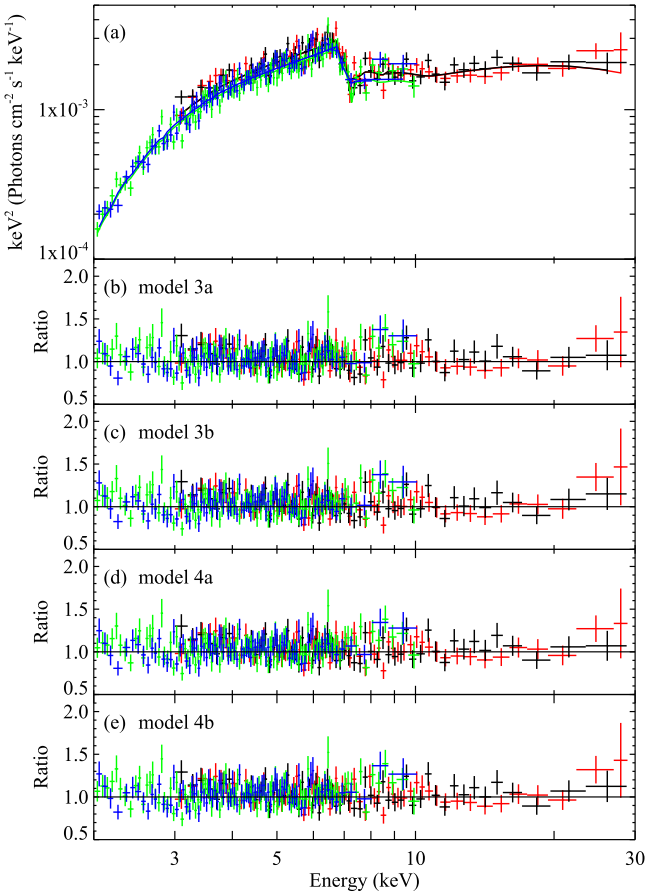

Figure 3. (a) *XMM-Newton* and *NuSTAR* spectra of IRAS 05189–2524 with the relativistic disk reflection model 4b. (b)–(e) Data/model ratio plots after fitting for the disk reflection component under four different absorption scenarios: (b) one neutral absorber with a solar iron abundance; (c) one neutral absorber with a variable iron abundance; (b) one neutral absorber with a solar iron abundance plus one ionized absorber; (c) one neutral absorber with a variable iron abundance plus one ionized absorber. The data are rebinned for display clarity. See Table 1 for the list of XSPEC models.

In an attempt to further constrain the iron abundance, we tie the iron abundances of the neutral absorber and the disk reflection component by replacing the `zpcfabs` model with an improved model for neutral absorption `tbnew_feo`[12] convolved with the partial covering model `partcov` (model 3b; see Table 1). Both Fe and O abundances are variable parameters in the `tbnew_feo` model. We freeze the O abundance at solar, since it would not have a significant influence on our spectral fitting above 2 keV. As a result, the model finds a best-fit iron abundance $A_{\rm Fe} = 5.5^{+2.5}_{-1.1}$, which is consistent with the measurement from Westmoquette et al. (2012). This model provides a slightly better fit for the data ($\chi^2/\mathrm{dof} = 860.6/859$), with a higher coronal height $h = 4.70^{+4.04}_{-1.99}$, a less steep power-law

[10] The ionization parameter $\xi = 4\pi F_x/n$, where F_x is the ionizing flux and n is the gas density.

[11] Only an upper limit was put on the metallicity because the line ratios were outside the range predicted by the photoionization, shock, or AGN models used in the paper.

[12] http://pulsar.sternwarte.uni-erlangen.de/wilms/research/tbabs/

continuum ($\Gamma = 1.79^{+0.17}_{-0.14}$), and a cutoff at 34^{+21}_{-10} keV, even lower than in the previous model. As a result, the reflection fraction is reduced to $R_{\rm ref} = 1.99$. We note here that the cutoff energy is uncommonly low for an AGN, even compared with the lowest *NuSTAR* measurements (e.g., Baloković et al. 2015; Ursini et al. 2015; Tortosa et al. 2016). This model generally has more uncertainty in the parameters; most notably, it places no constraint on the BH spin. Although the metallicities in the whole galaxy should be related, there is no solid justification to assume that the metallicities are the same in the BH vicinity and in the outer disk of the galaxy. However, we believe that it is a reasonable simplification given the data quality; untying the iron abundances brings no obvious improvement to the fitting.

Given the possible ionized absorption features in the Fe K band and motivated by the presence of large-scale outflows in the host galaxy (e.g., Westmoquette et al. 2012; Bellocchi et al. 2013; Rupke & Veilleux 2015), we add an ionized absorption component to account for any outflowing ionized absorbers. We modify the spectrum with an ionized absorption table model calculated by the XSTAR code (Kallman & Bautista 2001) and tie its iron abundance with that of the `relxilllp` component. It is a physically reasonable requirement, since if the wind has extreme velocity, it most likely arises from the accretion disk; thus, the same chemical abundances would naturally be expected. We first assume that the partial covering neutral absorber has a solar iron abundance (model 4a; see Table 1). The fitting results reveal an ionized absorber with a velocity $v_{\rm out} = 0.13^{+0.02}_{-0.06}\,c$ in the source rest frame, which is well above the typical outflowing velocities of warm absorbers, about the common value found for UFOs (e.g., Tombesi et al. 2010). With an ionization parameter $\log \xi = 3.06 \pm 0.07$ erg cm s^{-1}, the absorption should be dominated by Fe XXV. However, the detection of a high-velocity ionized outflow is not significant, as it only brings marginal improvement to the fitting, $\Delta\chi^2/\Delta{\rm dof} = -7.2/-3$, and the difference is not visually evident in the ratio plot. Other best-fit parameters are consistent with model 3a (without the ionized absorber). A rapidly spinning BH with $a > 0.89$ is required to provide an adequate fit for the data.

We then reintroduce the neutral absorption model with a variable iron abundance (model 4b; see Table 1) and force the iron abundances of the disk reflection, the outflowing wind, and the neutral absorber to be the same. The model brings no further improvement for the fitting. But again, it reduces the iron abundance $A_{\rm Fe}$ to $\sim$5, and since the iron abundance and the column density in the XSTAR model are degenerate parameters, the column density of the ionized outflow is estimated to be higher. Best-fit parameters of the disk reflection agree well with those given by model 3b, except for a slightly higher inclination of $\theta = 51^{+4}_{-5}{}^{\circ}$. Only a low BH spin can be ruled out at the 90% confidence level by this model.

4. Discussion

We test four models under different absorption scenarios to physically fit for the disk reflection features in IRAS 05189–2524, which provide good and comparable fits to the 2–30 keV broadband spectrum (for details, see Table 3 and Figure 3). With the covering fraction of the neutral absorber fixed at 99%, there is also no large discrepancy in the continuum below 2 keV. Based on the limited S/N of the spectrum, we cannot distinguish which model better describes the data. A supersolar neutral absorber is a reasonable requirement by the metallicity measurement of the galaxy from the literature, and it reduces the disk iron abundance to a less extreme value. However, detailed modeling of the intrinsic absorption causes apparent difficulty in disentangling the parameter degeneracies. Adding an ionized absorber modeled by XSTAR helps to account for the possible features of a high-velocity outflow in the Fe K band, but it is not statistically strongly required. For three out of the four models, we can rule out a slow or retrograde BH spin at the 90% confidence level. In models 3a and 4a, a rapidly spinning BH is favored (for the spin constraints, see Figure 4). In addition, we consider the possible contribution from distant reflection produced in the torus or BLR, but including an extra `xillver` component does not improve the fitting.

4.1. Supersolar Iron Abundance

In our spectral analysis of IRAS 05189–2524, all acceptable fits require a supersolar iron abundance for the disk reflection component, but the value is not very well constrained. The primary effect of the iron abundance parameter is to change the relative strength of the iron line and the Compton hump. Because of the low net number counts at the high-energy end of the *NuSTAR* spectra, the shape of the Compton hump is not well constrained, which could make it difficult to obtain a tight constraint of the iron abundance. We note that a similar overabundance in iron has been reported in a number of AGNs (e.g., Risaliti et al. 2009; Patrick et al. 2011) and stellar-mass BHs (e.g., García et al. 2015b), with the examples of well-known narrow-line Seyfert 1 galaxies (NLSy1s) 1H 0707–495 (Dauser et al. 2012; Kara et al. 2015) and IRAS 13224–3809 (Fabian et al. 2013). In the case of IRAS 05189–2524, the galaxy is undergoing intense star formation, so it is expected to be iron enriched. Since supersolar metallicities were indicated via spatially resolved optical spectroscopy in the outer disk and the nuclear region of the galaxy (Westmoquette et al. 2012), it is physically reasonable for the iron abundance to be high in the accretion disk.

4.2. Absorption-dominated Models

Absorption from material lying relatively distant from the BH has frequently been proposed as an alternative interpretation of relativistic disk reflection (e.g., Miller et al. 2008, 2009). To investigate whether the excesses in the Fe K band and above 10 keV observed in IRAS 05189–2524 can be fully accounted for by absorption-dominated models (without the reflection component), we test modeling the 2–30 keV spectrum with single and dual partial covering neutral absorption models with variable iron abundances. For the single-absorber model,[13] we fix the covering faction at 99% to avoid large deviation from the data below 2 keV, the same way as in all the previous modelings. With $\Delta\chi^2 = 215.6$ compared to model 3b, this scenario can be easily ruled out. The dual-absorber model[14] with an iron abundance $A_{\rm Fe} = 2.2^{+0.2}_{-0.4}$ provides a better fit for the data, which requires one full covering absorber with the column density $N_{\rm H,abs\,1} = 6.01^{+0.14}_{-0.93} \times 10^{22}$ cm^{-2} and another of the coverage fraction $f_{\rm abs\,2} = 64\% \pm 5\%$ with $N_{\rm H,abs\,2} = 1.92^{+0.58}_{-0.18} \times 10^{23}$ cm^{-2}. However, it is still statistically worse than the reflection-

[13] (partcov*tbnew_feo)*powerlaw.
[14] (partcov*tbnew_feo)*(partcov*tbnew_feo)*powerlaw.

Table 3
Spectral Fitting of IRAS 05189–2524: Self-consistent Disk Reflection Models

Component	Parameter	Model 3a	Model 3b	Model 4a	Model 4b
ZPCFABS	$N_{\rm H}$ ($\times 10^{22}$ cm^{-2})	$7.17^{+0.17}_{-0.16}$	$4.20^{+0.21}_{-0.27}$	$7.15^{+0.62}_{-0.53}$	$4.33^{+0.98}_{-0.33}$
	$f_{\rm abs}$ (%)	99*	99*	99*	99*
	$A_{\rm Fe}$	…	$5.5^{+2.5}_{-1.1}$	…	$5.0^{+u}_{-0.7}$
XSTAR	$N_{\rm H}$ ($\times 10^{22}$ cm^{-2})	…	…	$0.27^{+0.37}_{-0.27}$	$1.44^{+1.56}_{-1.44}$
	log ξ (erg cm s^{-1})	…	…	$3.20^{+1.26}_{-0.68}$	$3.17^{+0.28}_{-0.39}$
	$V_{\rm out}$ (c)	…	…	$0.13^{+0.02}_{-0.06}$	$0.12^{+0.02}_{-0.01}$
	$A_{\rm Fe}$	…	…	$10.0^{+u}_{-3.3}$	$5.0^{+u}_{-0.7}$
RELXILLLP	h (GM/c^2)	$2.39^{+0.80}_{-0.32}$	$4.70^{+4.04}_{-1.99}$	$3.00^{+1.48}_{-0.87}$	$4.08^{+2.16}_{-1.60}$
	a (cJ/GM^2)	$0.96^{+0.02}_{-0.03}$	$0.96^{+u}_{-0.94}$	$0.96^{+u}_{-0.07}$	$0.98^{+u}_{-0.61}$
	θ (°)	42 ± 2	44^{+2}_{-5}	41^{+5}_{-2}	51^{+4}_{-5}
	Γ	$2.04^{+0.02}_{-0.03}$	$1.79^{+0.17}_{-0.14}$	$2.00^{+0.17}_{-0.19}$	$1.74^{+0.18}_{-0.17}$
	log ξ (erg cm s^{-1})	3.02 ± 0.02	$3.12^{+0.22}_{-0.11}$	3.06 ± 0.07	$3.23^{+0.14}_{-0.18}$
	$A_{\rm Fe}$	$10.0^{+u}_{-1.3}$	$5.5^{+2.5}_{-1.1}$	$10.0^{+u}_{-3.3}$	$5.0^{+u}_{-0.7}$
	$E_{\rm cut}$ (keV)	55^{+10}_{-7}	34^{+21}_{-10}	59^{+111}_{-24}	33^{+21}_{-10}
	χ^2/dof	862.0/859	860.6/859	854.8/856	854.7/856

Note. Models 3–4 fit the broadband spectrum with the part below 2.0 keV ignored. Parameters with an asterisk are fixed values. Iron abundances ($A_{\rm Fe}$) are linked during the spectral fitting. Values with uncertainty marked with $+u$ denote 90% confidence limits in excess of the upper bound of the model.

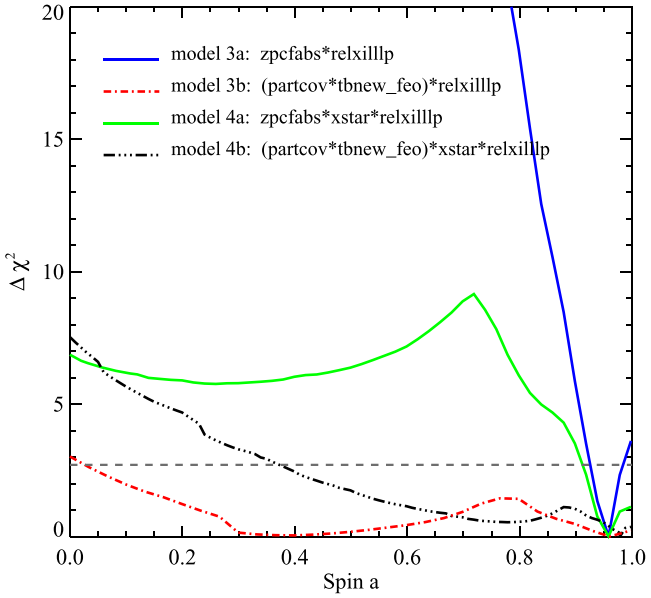

Figure 4. $\Delta\chi^2$ as a function of BH spin for the relativistic disk reflection modeling under four different absorption scenarios. The dashed line marks the 90% confidence limit. Models 3a and 4a favor a high BH spin of $\gtrsim$0.9. The constraint weakens considerably when we consider a variable iron abundance for the neutral absorber in models 3b and 4b.

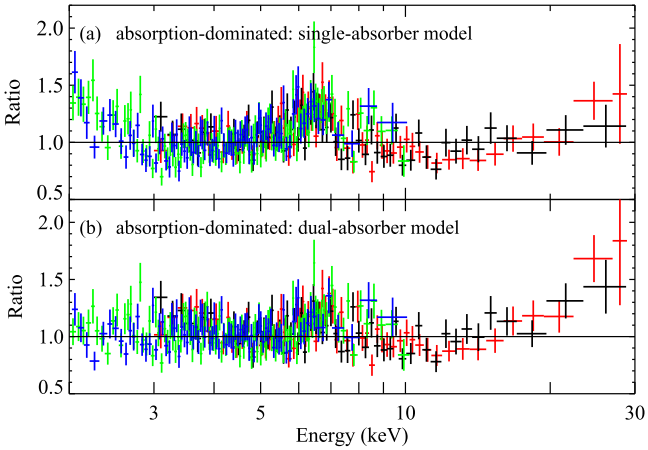

Figure 5. Data/model ratio plots of the absorption-dominated models: (a) one neutral partial covering absorber with the covering fraction fixed at 99% and a variable iron abundance; (b) two partial covering absorbers of free covering fractions and linked iron abundances. The data are rebinned for display clarity.

dominated model with $\Delta\chi^2 = 75.6$. The model leaves a broad excess in the Fe K band and also fails to produce the shape of the Compton hump above 10 keV (see Figure 5(b)), resembling the case in NGC 1365 (Risaliti et al. 2013).

4.3. Eddington Ratio and Outflow

The time-averaged 2–30 keV X-ray flux observed by *NuSTAR* is 7.1×10^{-12} erg cm^{-2} s^{-1}, corresponding to an intrinsic luminosity of 3.0×10^{43} erg s^{-1} during the 2013 observation. Using the central velocity dispersions measured from the Ca II triplet line widths (Rothberg et al. 2013) and the $M_{\rm BH}$–σ relation (Tremaine et al. 2002), the BH mass of IRAS 05189–2524 is estimated to be $M_{\rm BH} = 4.2 \times 10^8\,M_\odot$. We note that the BH mass derived from the Ca II triplet here is more than 10 times larger than the value measured from CO bandheads in the near-infrared (Dasyra et al. 2006). As discussed in Dasyra et al. (2006), CO bandheads are often representative of young stellar populations, which could lead to systematically lower BH masses for ULIRGs. Combined with the bolometric luminosity inferred from the infrared (Teng et al. 2015), IRAS 05189–2524 is measured to be accreting at an Eddington rate $\lambda_{\rm Edd} = L_{\rm bol}/L_{\rm Edd}$ of 0.12. Based on the correlation between the photon indices and the Eddington ratios of AGNs (Shemmer et al. 2008; Brightman et al. 2013, 2016), a photon index of $\Gamma \sim 2.0$ would be expected. The photon index obtained by our disk reflection modeling with a low cutoff

energy is $\Gamma \simeq 1.7$–2.0, which is consistent with the expected value given the scatter of the relation.

In our spectral modeling, we did not detect significant disk winds. Fitting the possible absorption features in the spectrum with a simple Gaussian absorption line using the `gabs` model would reach similar χ^2 to the physical XSTAR grid, with the best-fit line centroid at ∼7.33 keV. Although the effect of this ionized absorber on the continuum is subtle, we include it in the spectral fitting, as even mild absorption lying around the Fe K edge could influence the BH spin measurement, which is sensitive to the profile of the broad iron line. The power of an outflow scales with the amount of matter being ejected (King & Pounds 2015). With the rather small column density measured for the ionized absorption compared with that of massive disk winds found in other AGNs (e.g., IRAS 11119+3257; Tombesi et al. 2015), even if a UFO indeed exists in IRAS 05189–2524 at the epoch of the observation, it is probably not energetic enough to have a large impact on its galactic environment.

5. Summary and Conclusion

We detect disk reflection features of a broad iron line and a Compton reflection hump in IRAS 05189–2524, a Seyfert 1h galaxy and ULIRG, from the *NuSTAR* and *XMM-Newton* data taken in 2013. With the broadband X-ray spectrum, an alternative dual partial covering absorber explanation can be ruled out. Physically modeling with the self-consistent relativistic reflection model `relxilllp` finds that the reflection is likely to be generated from the inner range of a rapidly spinning BH. The high reflection fraction measured ($R_{\rm ref} \simeq 2.0$–3.2) indicates that the reflection area is close to the BH, where relativistic light-bending effects boost the reflection signature (Miniutti & Fabian 2004), suggesting that the coronal illuminating source is compact. However, due to the complex effects from neutral and ionized absorption and the limited S/N data, parameter degeneracies preclude putting a tight, model-independent estimation on the BH spin.

As a merger system, IRAS 05189–2524 is an interesting target for the spin measurement, as BH spins are believed to encode information about the galaxy evolution history (Berti & Volonteri 2008), and ULIRGs have been proposed as an important transition phase in the hierarchical evolution model of galaxies (Sanders et al. 1988; Hopkins et al. 2006). Simulations predict that it is uncommon for mergers to yield large spins, unless alignment of the spins of the merging BHs with the orbital angular momentum is very efficient (Berti & Volonteri 2008).

With Fe K band absorption features marginally evident in the residuals, the detection of a high-velocity ionized wind is not statistically significant. Also, we find that the iron abundance of the neural absorber is strongly degenerated with the BH spin. Future observations with higher-S/N data could help disentangle the reflection component from the underlying continuum and the various absorption effects. Assuming that the source remains at the flux level observed in 2013, if the ionized absorption indeed exists in IRAS 05189–2524, simulations indicate that the XSTAR component would be significantly required by data sets with more than ∼2 times the exposure, leading to a $>3\sigma$ detection of the ionized absorption features. With longer observations (500 ks *NuSTAR* and 300 ks *XMM-Newton* exposures), it would be possible to obtain the BH spin to within ∼30% of uncertainty under all the different absorption scenarios we have discussed above.

We thank the anonymous referee for helpful comments that improved the paper. M.B. acknowledges support from NASA Headquarters under the NASA Earth and Space Science Fellowship Program, grant NNX14AQ07H. This work was supported under NASA Contract no. NNG08FD60C and made use of data obtained with *NuSTAR*, a project led by Caltech, funded by NASA, and managed by NASA/JPL, and has utilized the NUSTARDAS software package, jointly developed by the ASDC (Italy) and Caltech (USA). We thank the *NuSTAR* Operations, Software and Calibration teams for support with the execution and analysis of these observations. This research has also made use of data obtained with *XMM-Newton*, an ESA science mission with instruments and contributions directly funded by ESA Member States.

References

Arnaud, K. A. 1996, in ASP Conf. Ser. 101, Astronomical Data Analysis Software and Systems V, ed. G. H. Jacoby & J. Barnes (San Francisco, CA: ASP), 17
Baloković, M., Matt, G., Harrison, F. A., et al. 2015, ApJ, 800, 62
Bellocchi, E., Arribas, S., Colina, L., & Miralles-Caballero, D. 2013, A&A, 557, A59
Berti, E., & Volonteri, M. 2008, ApJ, 684, 822–8
Brightman, M., Masini, A., Ballantyne, D. R., et al. 2016, ApJ, 826, 93
Brightman, M., & Nandra, K. 2011, MNRAS, 413, 1206
Brightman, M., Silverman, J. D., Mainieri, V., et al. 2013, MNRAS, 433, 2485
Dasyra, K. M., Tacconi, L. J., Davies, R. I., et al. 2006, ApJ, 651, 835
Dauser, T., García, J., Parker, M. L., Fabian, A. C., & Wilms, J. 2014, MNRAS, 444, L100
Dauser, T., Garcia, J., Wilms, J., et al. 2013, MNRAS, 430, 1694
Dauser, T., Svoboda, J., Schartel, N., et al. 2012, MNRAS, 422, 1914
Fabian, A. C., Kara, E., Walton, D. J., et al. 2013, MNRAS, 429, 2917
Fabian, A. C., Rees, M. J., Stella, L., & White, N. E. 1989, MNRAS, 238, 729
Feruglio, C., Fiore, F., Carniani, S., et al. 2015, A&A, 583, A99
García, J., Dauser, T., Lohfink, A., et al. 2014, ApJ, 782, 76
García, J. A., Dauser, T., Steiner, J. F., et al. 2015a, ApJL, 808, L37
García, J. A., Steiner, J. F., McClintock, J. E., et al. 2015b, ApJ, 813, 84
George, I. M., & Fabian, A. C. 1991, MNRAS, 249, 352
Haardt, F., & Maraschi, L. 1993, ApJ, 413, 507
Harrison, F. A., Craig, W. W., Christensen, F. E., et al. 2013, ApJ, 770, 103
Hopkins, P. F., Hernquist, L., Cox, T. J., et al. 2006, ApJS, 163, 1
Iwasawa, K., Fabian, A. C., Mushotzky, R. F., et al. 1996, MNRAS, 279, 837
Jansen, F., Lumb, D., Altieri, B., et al. 2001, A&A, 365, L1
Kalberla, P. M. W., Burton, W. B., Hartmann, D., et al. 2005, A&A, 440, 775
Kallman, T., & Bautista, M. 2001, ApJS, 133, 221
Kara, E., Fabian, A. C., Lohfink, A. M., et al. 2015, MNRAS, 449, 234
King, A., & Pounds, K. 2015, ARA&A, 53, 115
Laor, A. 1991, ApJ, 376, 90
Lehmer, B. D., Alexander, D. M., Bauer, F. E., et al. 2010, ApJ, 724, 559
Madsen, K. K., Harrison, F. A., Markwardt, C. B., et al. 2015, ApJS, 220, 8
Magdziarz, P., & Zdziarski, A. A. 1995, MNRAS, 273, 837
Miller, L., Turner, T. J., & Reeves, J. N. 2008, A&A, 483, 437
Miller, L., Turner, T. J., & Reeves, J. N. 2009, MNRAS, 399, L69
Miniutti, G., & Fabian, A. C. 2004, MNRAS, 349, 1435
Murphy, K. D., & Yaqoob, T. 2009, MNRAS, 397, 1549
Nandra, K., O'Neill, P. M., George, I. M., & Reeves, J. N. 2007, MNRAS, 382, 194
Nandra, K., & Pounds, K. A. 1994, MNRAS, 268, 405
Nardini, E., Reeves, J. N., Gofford, J., et al. 2015, Sci, 347, 860
Patrick, A. R., Reeves, J. N., Lobban, A. P., Porquet, D., & Markowitz, A. G. 2011, MNRAS, 416, 2725
Pounds, K. A., & King, A. R. 2013, MNRAS, 433, 1369
Pounds, K. A., King, A. R., Page, K. L., & O'Brien, P. T. 2003, MNRAS, 346, 1025
Ricci, C., Tazaki, F., Ueda, Y., et al. 2014, ApJ, 795, 147
Risaliti, G., Harrison, F. A., Madsen, K. K., et al. 2013, Natur, 494, 449
Risaliti, G., Miniutti, G., Elvis, M., et al. 2009, ApJ, 696, 160
Rivers, E., Markowitz, A., & Rothschild, R. 2013, ApJ, 772, 114
Rothberg, B., Fischer, J., Rodrigues, M., & Sanders, D. B. 2013, ApJ, 767, 72
Rupke, D. S., Veilleux, S., & Sanders, D. B. 2005, ApJ, 632, 751
Rupke, D. S. N., & Veilleux, S. 2015, ApJ, 801, 126
Rupke, D. S. N., Veilleux, S., & Baker, A. J. 2008, ApJ, 674, 172

Sanders, D. B., Soifer, B. T., Elias, J. H., et al. 1988, ApJ, 325, 74
Severgnini, P., Risaliti, G., Marconi, A., Maiolino, R., & Salvati, M. 2001, A&A, 368, 44
Shemmer, O., Brandt, W. N., Netzer, H., Maiolino, R., & Kaspi, S. 2008, ApJ, 682, 81
Strüder, L., Briel, U., Dennerl, K., et al. 2001, A&A, 365, L18
Tan, Y., Wang, J. X., Shu, X. W., & Zhou, Y. 2012, ApJL, 747, L11
Tanaka, Y., Nandra, K., Fabian, A. C., et al. 1995, Natur, 375, 659
Teng, S. H., Rigby, J. R., Stern, D., et al. 2015, ApJ, 814, 56
Teng, S. H., Veilleux, S., Anabuki, N., et al. 2009, ApJ, 691, 261
Teng, S. H., Veilleux, S., & Baker, A. J. 2013, ApJ, 765, 95
Tombesi, F., Cappi, M., Reeves, J. N., et al. 2010, A&A, 521, A57
Tombesi, F., Meléndez, M., Veilleux, S., et al. 2015, Natur, 519, 436
Tortosa, A., Marinucci, A., Matt, G., et al. 2016, arXiv:1612.05871
Tremaine, S., Gebhardt, K., Bender, R., et al. 2002, ApJ, 574, 740
Turner, M. J. L., Abbey, A., Arnaud, M., et al. 2001, A&A, 365, L27
Ursini, F., Boissay, R., Petrucci, P.-O., et al. 2015, A&A, 577, A38
Veilleux, S., Kim, D.-C., Sanders, D. B., Mazzarella, J. M., & Soifer, B. T. 1995, ApJS, 98, 171
Veilleux, S., Meléndez, M., Sturm, E., et al. 2013, ApJ, 776, 27
Veilleux, S., Sanders, D. B., & Kim, D.-C. 1999, ApJ, 522, 139
Véron-Cetty, M.-P., & Véron, P. 2006, A&A, 455, 773
Vivian, U., Sanders, D. B., Mazzarella, J. M., et al. 2012, ApJS, 203, 9
Walton, D. J., Nardini, E., Fabian, A. C., Gallo, L. C., & Reis, R. C. 2013, MNRAS, 428, 2901
Walton, D. J., Risaliti, G., Harrison, F. A., et al. 2014, ApJ, 788, 76
Westmoquette, M. S., Clements, D. L., Bendo, G. J., & Khan, S. A. 2012, MNRAS, 424, 416
Wilms, J., Allen, A., & McCray, R. 2000, ApJ, 542, 914
Winter, L. M., Mushotzky, R. F., Reynolds, C. S., & Tueller, J. 2009, ApJ, 680, 1322
Young, S., Hough, J. H., Efstathiou, A., et al. 1996, MNRAS, 281, 1206